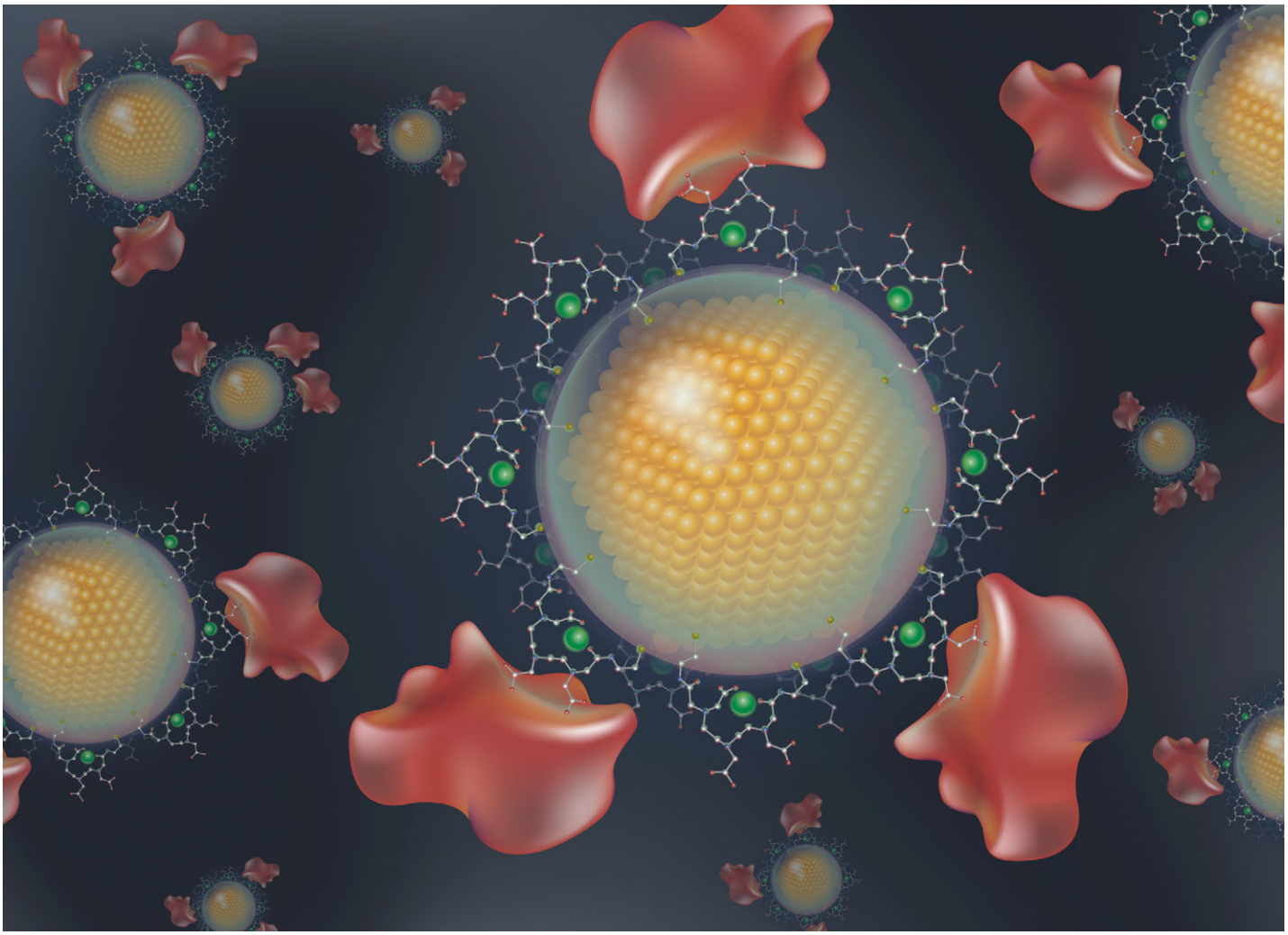

Showcasing research from Raghuraman Kannan's Laboratory/Department of Radiology, University of Missouri, Columbia, MO, USA

Synthesis and characterization of functional multicomponent nanosized gallium chelated gold crystals

A novel synthetic method for fabricating multicomponent gold nanoparticles containing both gallium ions and biomolecules promises clinical benefits for molecular imaging. This research has developed a [AuNP(DTDTPA)(Ga)] conjugate, that is emerging as a promising platform for developing biologically useful MCNs to help detect and treat human diseases.

As featured in:

See Raghuraman Kannan *et al.*, *Chem. Commun.*, 2014, **50**, 3281.

ROYAL SOCIETY OF CHEMISTRY

www.rsc.org/chemcomm

Registered charity number: 207890

ChemComm

COMMUNICATION

View Article Online
View Journal | View Issue

Cite this: *Chem. Commun.*, 2014, **50**, 3281

Received 24th September 2013,
Accepted 12th January 2014

DOI: 10.1039/c3cc47308b

www.rsc.org/chemcomm

Synthesis and characterization of functional multicomponent nanosized gallium chelated gold crystals†

Ajit Zambre,‡[a] Francisco Silva,‡[b] Anandhi Upendran,[c] Zahra Afrasiabi,[d] Yan Xin,[e] António Paulo[b] and Raghuraman Kannan*[afg]

In this communication, we describe a novel synthetic method for fabricating multicomponent gold nanoparticles containing both gallium ions and biomolecules on the surface. Detailed compositional analysis, using STEM-HAADF and EELS spectroscopy, confirmed the crystalline nature of gold and chelation of gallium ions. The presence of the biomolecule was validated using conventional ELISA.

Design and synthesis of multicomponent nanomaterials (MCNs) have attracted significant research interest owing to their promising applications in the field of medicine.[1,2] MCNs combine physical and biological properties of multiple materials within a single nanoconstruct. Such combinations provide unique opportunities in simultaneous detection and treatment of various human diseases.[1] On the other hand, design of multiple components within a single platform poses significant challenges in the synthesis and characterization of these nanomaterials.[3] Nevertheless, it is vital to ensure that each nanoparticle comprises materials of the desired composition and the inherent properties are retained to obtain the expected clinical benefits.[4] Indeed, we focused our research on addressing important challenges, including synthesis, precise atomic level identification, quantification, and characterization, in the fabrication of gold nanoparticle (AuNP) based MCNs. Specifically, in this communication, we report the synthesis and detailed characterization of MCNs of formula [AuNP(Ga)(HRP)]; (HRP = Horseradish peroxidase). The rationale for choosing these components in our MCN design is as follows: (i) AuNPs possess significant advantages including a rich surface chemistry, non-toxic behavior, and non-immunogenic characteristics;[4,5] (ii) Ga-67 and Ga-68 are gamma and positron emitting isotopes respectively, and are widely used in molecular imaging;[6] and (iii) HRP serves as a model biomolecule and its presence can be confirmed using conventional ELISA techniques.[7]

In our MCN design, we used AuNPs conjugated with an amino-carboxylate ligand (diethylene triamine pentaacetic acid, DTPA) on the surface *via* dithiol (DT) linkage (AuNP-DTDTPA).[8–10] Pioneering efforts by Roux and coworkers have shown that AuNP-DTDTPA is an excellent platform for conjugation with Gd, In, or ^{99m}Tc, and these elements have excellent molecular imaging capabilities.[8–10] Dithiolated DTPA (DTDTPA) has several unique advantages such as a smaller bite-size, and the presence of both soft N-donor and hard O-donor ligands.[8,9] Unlike other N, O-ligands, DTPA forms kinetically inert and thermodynamically stable metal complexes under normal laboratory conditions. DTPA based metal chelates have shown excellent *in vivo* stability.[10,11] Such characteristic features of DTPA bring numerous potential clinical benefits for *in vivo* imaging.[11] For these reasons, the [AuNP(DTDTPA)] (**1**) conjugate is emerging as a promising platform for developing biologically useful MCNs. As part of our ongoing studies in the design and development of gold nanoparticles,[12,13] we report (i) the synthesis of [AuNP(DTDTPA)(Ga)] (**2**), (Scheme 1); (ii) characterization of **2** using advanced Scanning Transmission Electron Microscopy (STEM) techniques; (iii) detailed *in vitro* stability and cytotoxicity

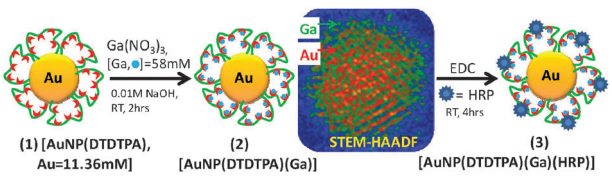

Scheme 1 Synthesis of **2** and **3**.

[a] *Department of Radiology, University of Missouri-Columbia, Columbia, Missouri-65212, USA. E-mail: kannanr@health.missouri.edu; Tel: +1 573 882 5676*
[b] *Centro de Ciências e Tecnologias Nucleares, Instituto Superior Técnico, Estrada Nacional 10 (Km 139,7), 2695-066 Bobadela LRS, Portugal*
[c] *Department of Physics, University of Missouri-Columbia, Columbia, Missouri-65212, USA*
[d] *Department of Life and Physical Sciences, Lincoln University, Jefferson City, Missouri 65101, USA*
[e] *National High Magnetic Field Laboratory, Florida State University, Tallahassee, FL 32310, USA*
[f] *Department of Bioengineering, University of Missouri-Columbia, Columbia, Missouri-65212, USA*
[g] *International Center for Nano/Micro Systems and Nanotechnology, University of Missouri-Columbia, Columbia, Missouri-65212, USA*

† Electronic supplementary information (ESI) available. See DOI: 10.1039/c3cc47308b

‡ These authors contributed equally.

studies of **2**; and (iv) the synthesis and characterization of [AuNP(DTDTPA)(Ga)(HRP)] (**3**).

We began our investigation by understanding the structural and physicochemical properties of **1**. Specifically, we were interested in understanding the integrity of the multi-layered carboxylate structure of **1** at various pH and dilutions (see ESI†). The layered carboxylate structure is crucial for attachment of different components. Our intent was to utilize carboxylate layers for both metal and biomolecule conjugation. Our detailed studies confirmed that the multilayered carboxylate architecture is fairly stable over a wide range of pH (6 to 13) and at different concentrations (30 μg ml^{-1} to 5 mg ml^{-1}).

[AuNP(DTDTPA)(Ga)] (**2**) was synthesized by treating **1** with $Ga(NO_3)_3$ at pH 8.0 (Scheme 1). The optimized ratio of Au : Ga is found to be 1 : 5. Complex **2** exhibits a core size of ~3 to 5 nm, hydrodynamic size of 88 nm and zeta potential of −55 mV. In order to investigate the maximum concentration of gallium that can be incorporated within the nanoconstruct (**1**) we performed serial titrations of **1** with Ga^{3+} and evaluated the resultant conjugate using both Ga-71 NMR spectroscopy and ICP-OES analysis (ESI,† Fig. S1). The NMR active ^{71}Ga is used as a probe to determine the concentration of chelated Ga. NMR spectra of different concentrations of $Ga(NO_3)_3$ were recorded in D_2O (ESI,† Fig. S2). A standard curve using concentrations of non-chelated Ga *vs.* peak integration values were plotted. Using the plot, we determined that 11 mM of Au can irreversibly chelate up to 58 mM of Ga. This indicates that any gallium added beyond this concentration would not be chelated with AuNP-DTDTPA. The NMR results were validated by performing additional experiments using ICP-OES. In this experiment, we monitored Au/Ga ratios of the resultant conjugates after treatment of 11 mM of **1** (Au) with different amounts of Ga^{3+}. The Au/Ga ratio becomes a constant after addition of 58 mM of Ga^{3+}. By these experiments, we have demonstrated the exact concentration of Ga that can be irreversibly chelated to **1**. The smaller core size of **2** made the characterization quite challenging. We utilized multiple analytical tools (UV-Vis, TEM, DLS, XPS, EDX, HAADF, and EELS; see the ESI† for all characterization data) to obtain the structural details of **2**. Conventional techniques such as UV-Vis and TEM confirmed that the crystallinity of the gold core of **1** is retained after chelation with Ga. As the gold core size is less than 5 nm, the plasmon resonance (λ_{max}) showed a small hump at 520 nm before and after complexation.

Nanoconstruct **2** has been characterized by STEM in a probe corrected JEM-ARM200cF at 200 kV. The STEM high angle annular dark field (HAADF) *Z*-contrast images show the Au atoms in white contrasts in Fig. 1. From a lower magnification image (Fig. 1a), the AuNP size distribution can be obtained accurately since the contrast is reflecting the real size of the particles without any diffraction interference contrast. The AuNP shows three size categories, with the largest diameter of 3.77 ± 0.25 nm, the medium ones of 2.43 ± 0.27 nm, and the smallest ones of 1.15 ± 0.13 nm. The atomic structure of a typical crystalline AuNP is shown in Fig. 1b with a higher magnification. The nanoparticle denoted as A in Fig. 1b is projected along the [110] direction exhibiting a 5-fold twinning structure. The smaller particle B does not show

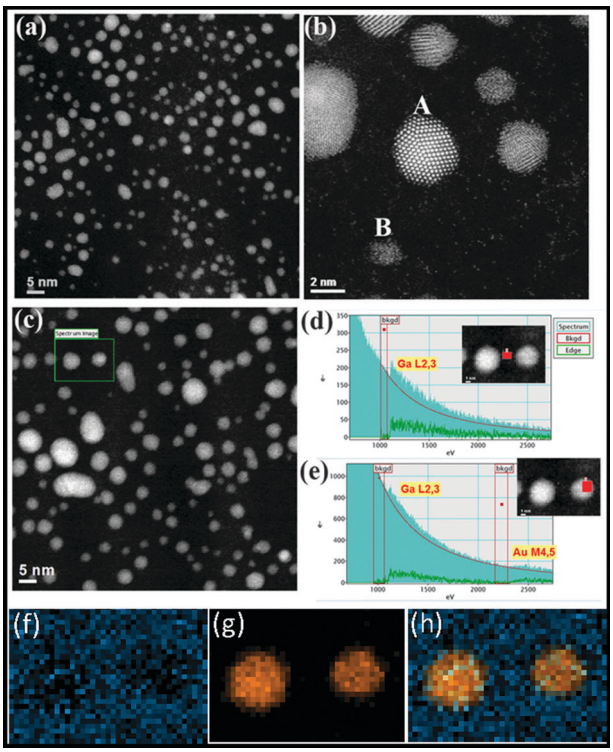

Fig. 1 The STEM-HAADF *Z*-contrast images of **2** showing the Au atoms in white contrasts. (a) Lower magnification image; (b) the atomic structures of a typical crystalline AuNP shown under high magnification; (c) HAADF view of the sample with a scanning region shown by the green outline; (d) EELS spectrum from a point between the two Au particles; (e) spectrum obtained from the top of the right AuNP showing presence of Ga; elemental mapping images of **2** showing (f) gallium emission; (g) gold emission; and (h) composite emission of Au and Ga distributions for two nanoparticles.

crystallinity, only forming a cluster of Au atoms. It is believed that the biggest AuNP particles were aggregated due to the irradiation of the electron beam. The white speckles seen in the dark background in the image are the scattered individual Au atoms. Some of the smallest clusters of AuNP are probably formed from these scattered Au atoms under the beam. This formation may be due to incident electron beam or beam induced heating (ESI,† Fig. S15). Similar effects have been observed in smaller gold clusters and are reported elsewhere.[14] Interestingly, we noted the movement of **2** under the electron beam (video clip uploaded in the ESI†). The lattice parameter of the AuNP has been deduced from the images of particles (similar to particle A), and it is measured to be 0.418 nm. It is larger than the Au bulk lattice parameter (0.408 nm). Since Ga atoms are much lighter than the Au atoms, where the HAADF image contrast is proportional to the atomic number $Z^{1.7}$, it is hard to discern the contrast of the Ga atoms in the amorphous carbon background in the HAADF image without quantitative experimental data. Therefore, the electron energy loss spectroscopy (EELS) and Spectrum Imaging (SI) techniques were used to detect the presence of the Ga in the samples as shown in Fig. 1c–e. Fig. 1c shows the HAADF view of the sample and the green box is the scanning region for SI, where core loss EELS spectra were collected on each pixel location of the scanned region.

Fig. 1d shows the EELS spectrum from a point between the two AuNP particles, and unmistakably shows the presence of Ga (L2,3 due to the core loss edge at 1115 eV). Fig. 1e presents the spectrum obtained from the top of the right AuNP. This spectrum clearly shows the presence of both Ga L2,3 (peak at 1115) and Au M4,5 (peak at 2206 eV), confirming the presence of Ga on the top of the AuNP. Overall, the SI data confirm that Ga is present and is surrounding the AuNP.

It is expected that the Ga^{3+} will effectively complex with carboxylate anions and amines closer to the surface of gold. The AuNP-DTDTPA-Ga structure was further analysed by XPS. Of particular interest to the present study is the binding of gallium to the surface ligand, DTDTPA. It is worth noting here that surface bound DTDTPA is rich in disulfides, secondary amines, and carboxylates. Even though the metallic alloy of Ga with Au is known to form at 400 °C, it is unexpected in the present scenario.[15,16] It is possible that Ga^{3+} can bind with thiol; however, thiols are present predominantly as disulfides in the parent nanoconstruct.[8,9] Such a binding would require oxidative addition of Ga^{3+} across disulfide bonds, which is not feasible based on the chemistry of gallium. However, N and O atoms present in the ligand are geometrically positioned to chelate with Ga. In conjugate **2**, the N(1S) levels showed a peak at 398.8 eV (ESI,† Fig. S16). Studies in the literature have demonstrated the N/S levels are not sensitive to these binding events.[14]

Having established the synthesis and characterization of the [AuNP(DTDTPA)Ga] (**2**) conjugate, we focused our attention to explore further utilization of carboxylate ligands on **2** for conjugating with biomolecules. As a proof-of-concept, we conjugated HRP to carboxylates on **2**. The presence of HRP was detected using the conventional ELISA technique.[7] We utilized two different conjugates of **2**, with varying amounts of Ga present in the nanoconjugate, namely, conjugates obtained after treatment of **1** with 29 mM of Ga and another one with the saturating amount of 58 mM. A low concentration of gallium (less than required for complete chelation) was used deliberately to increase the number of free carboxylates while a very high amount (more than that required for complete chelation) was used to utilize all possible carboxylates present in the nanoconstruct. The absorbance of conjugated HRP was plotted against the concentration of nanoconstruct (**2**) to relate the binding capabilities. Fig. 2 shows the absorbance of conjugated HRP with serial 10-fold dilutions of **2**. It was obvious that the absorbance increases with increasing concentration of **2** as the HRP holding capability of **2** increases. On the other hand, chelates with varying concentrations of Ga (29 mM and 58 mM) did not show any difference in conjugation with HRP (Fig. 2 *inset*). These data suggest that HRP conjugation with **2** is independent of the amount of chelated Ga.

Based on our analytical and microscopy data, it is fair to assume that HRP is conjugated with sterically less-crowded carboxylates that are available after gallium chelation on the nanoparticle. This could be due to the fact that the surface attached DTDTPA ligand would possibly exhibit two kinds of carboxylates on the surface; the first kind would be a part of the compact ligand structures that are ideally required for chelation

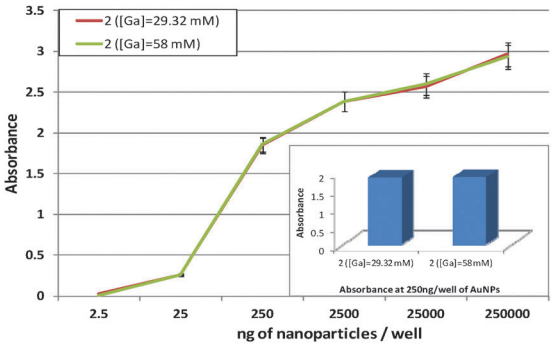

Fig. 2 ELISA binding plot of **2** with two concentrations (29.32 and 58.0 mM) of $Ga(NO_3)_3$ reacted with **1** for the determination of peroxidase activity; and *inset* shows carboxylate conjugation efficiency of **2** with HRP using ELISA.

of gallium and the second kind would be carboxylates that are not conformationally favourable for forming a thermodynamically stable metal chelate. The second kind of carboxylates is available for biomolecule conjugation. The possibility for interaction of gallium atoms with these conformationally unfavourable carboxylates is minimal. Due to this binding preference of gallium and HRP, we reason that HRP conjugation efficiency remains the same for both low (29 mM) and high (58 mM) gallium chelated AuNPs.

The cytotoxicities of **1** and **2** were studied on human prostate cancer (PC-3) cells under *in vitro* conditions using a colorimetric cell-viability (MTT) assay (ESI,† Fig. S7). The results demonstrate that nanoconstructs **1** and **2** do not show cytotoxicity up to 40 μg ml^{-1} concentrations. Nevertheless, the cell viability was slightly lesser for **2** than **1** for a period of 24 h post-treatment. It is worth mentioning here that AuNPs are non-toxic.[17] In addition, our studies showed that nanoconstruct **1**, containing a DTDTPA ligand coating on the surface of AuNPs, is non-toxic. Therefore, the minimal toxicity exhibited by **2** may be attributed to conjugated gallium. The lack of any noticeable toxicity of **1** and **2** thereby provides new opportunities for utilizing these conjugates for biomedical imaging.

We have demonstrated that **1** can serve as an ideal platform for synthesizing MCNs containing metal atoms and biomolecules. The presence of all three components, Au, Ga, and biomolecule in a single MCN has been confirmed using sophisticated analytical techniques. Such MCNs with radiolabeled metals can serve as a unique scaffold for conjugation of diverse biomolecules for specific targeting with molecular imaging capability.

R.K. acknowledges the Michael J. and Sharon R. Bukstein Faculty Professorship endowment on Cancer Research for financial support. Authors also acknowledge funding from USDA–NIFA (2011-02535), Coulter Translational Program Bridge award, MU iCATS Faculty Innovator Award, Fast Track Economic Development Award, and Mizzou Advantage award. Fundação para a Ciência e Tecnologia (FCT) is acknowledged for financial support (EXCL/QEQ-MED/0233/2012). F. Silva thanks FCT for the doctoral research grant (SFRH/BD/47308/2008). The EELS work was carried out at Florida State University (FSU) and the facility is funded and supported by the FSU Research Foundation, National High Magnetic Field Laboratory (NSF-DMR-0654118)

and the State of Florida. The authors acknowledge Dr Wen Ritts, Electron Microscopy Core Facility at the University of Missouri-Columbia.

Notes and references

1 D. A. Giljohann, D. S. Seferos, W. L. Daniel, M. D. Massich, P. C. Patel and C. A. Mirkin, Gold nanoparticles for biology and medicine, *Angew. Chem., Int. Ed.*, 2010, **49**(19), 3280–3294.
2 M. Ferrari, Cancer nanotechnology: opportunities and challenges, *Nat. Rev. Cancer*, 2005, **5**(3), 161–171.
3 D. Wang and Y. Li, Bimetallic nanocrystals: liquid-phase synthesis and catalytic applications, *Adv. Mater.*, 2011, **23**(9), 1044–1060.
4 N. Desai, Challenges in development of nanoparticle-based therapeutics, *AAPS J.*, 2012, **14**(2), 282–295.
5 A. C. Eifler and C. S. Thaxton, Nanoparticle therapeutics: FDA approval, clinical trials, regulatory pathways, and case study, *Methods Mol. Biol.*, 2011, **726**, 325–338.
6 C. R. Chitambar, Medical applications and toxicities of gallium compounds, *Int. J. Environ. Res. Public Health*, 2010, **7**(5), 2337–2361.
7 P. Samara, H. Kalbacher and K. Ioannou, *et al.*, Development of an ELISA for the quantification of the C-terminal decapeptide prothymosin alpha(100-109) in sera of mice infected with bacteria, *J. Immunol. Methods*, 2013, **395**(1-2), 54–62.
8 C. Alric, J. Taleb and G. Le Duc, *et al.*, Gadolinium chelate coated gold nanoparticles as contrast agents for both X-ray computed tomography and magnetic resonance imaging, *J. Am. Chem. Soc.*, 2008, **130**(18), 5908–5915.
9 P.-J. Debouttière, S. Roux, F. Vocanson, C. Billotey, O. Beuf, A. Favre-Réguillon, Y. Lin, S. Pellet-Rostaing, R. Lamartine, P. Perriat and O. Tillement, Design of Gold Nanoparticles for Magnetic Resonance Imaging, *Adv. Funct. Mater.*, 2006, **16**, 2330–2339.
10 C. Alric, I. Miladi and D. Kryza, *et al.*, The biodistribution of gold nanoparticles designed for renal clearance, *Nanoscale*, 2013, **5**(13), 5930–5939.
11 M. K. Moi, S. J. DeNardo and C. F. Meares, Stable bifunctional chelates of metals used in radiotherapy, *Cancer Res.*, 1990, **50**(3 suppl), 789s–793s.
12 N. Chanda, V. Kattumuri and R. Shukla, *et al.*, Bombesin functionalized gold nanoparticles show *in vitro* and *in vivo* cancer receptor specificity, *Proc. Natl. Acad. Sci. U. S. A.*, 2010, **107**(19), 8760–8765.
13 N. Chanda, R. Shukla, K. V. Katti and R. Kannan, Gastrin releasing protein receptor specific gold nanorods: breast and prostate tumor avid nanovectors for molecular imaging, *Nano Lett.*, 2009, **9**(5), 1798–1805.
14 Z. W. Wang and R. E. Palmer, Mass spectrometry and dynamics of gold adatoms observed on the surface of size-selected Au nanoclusters, *Nano Lett.*, 2012, **12**(1), 91–95.
15 M. M. Yazdanpanah, S. A. Harfenist and R. W. Cohn, Gallium-driven assembly of gold nanowire networks, *Appl. Phys. Lett.*, 2004, **85**(9), 1592–1594.
16 V. G. Weizer and N. S. Fatemi, The interaction of gold with gallium arsenide, *J. Appl. Phys.*, 1988, **64**(9), 4618–4623.
17 E. E. Connor, J. Mwamuka, A. Gole, C. J. Murphy and M. D. Wyatt, *Small*, 2005, **1**, 325–327.

